INSTITUTE OF PHYSICS PUBLISHING JOURNAL OF MICROMECHANICS AND MICROENGINEERING

J. Micromech. Microeng. **15** (2005) 1406–1413 doi:10.1088/0960-1317/15/8/005

Fabrication and characterization of diamond-like carbon/Ni bimorph normally closed microcages

J K Luo[1], J H He[1], Y Q Fu[1], A J Flewitt[1], S M Spearing[2,3], N A Fleck[1] and W I Milne[1]

[1] Department of Engineering, University of Cambridge, Trumpington Street, Cambridge, CB2 1PZ, UK
[2] Department of Aeronautics & Astronautics, MIT, Cambridge, MA 02139, USA
[3] School of Engineering Science, University of Southampton, Southampton, SO17 1QJ, UK

Received 13 January 2005, in final form 21 April 2005
Published 25 May 2005
Online at stacks.iop.org/JMM/15/1406

Abstract

Normally closed microcages based on highly compressively stressed diamond-like carbon (DLC) and electroplated Ni bimorph structures have been simulated, fabricated and characterized. Finite-element and analytical models were used to simulate the device performance. It was found that the radius of curvature of the bimorph layer can be adjusted by varying the DLC film stress, the total layer thickness and the thickness ratio of the DLC to Ni layers. The angular deflection of the bimorph structures can also be adjusted by varying the finger length. The radius of curvature of the microcage was in the range of 18–50 μm, suitable for capturing and confining micro-objects with sizes of 20–100 μm. The operation of this type of device is very efficient due to the large difference in thermal expansion coefficients of the DLC and the Ni layers. Electrical tests have shown that these microcages can be opened by $\sim 90^\circ$ utilizing a power smaller than 20 mW. The operating temperatures of the devices under various pulsed currents were extracted through the change in electrical resistance of the devices. The results showed that an average temperature in the range of 400–450 °C is needed to open this type of microcage by $\sim 90^\circ$, consistent with the results from analytical simulation and finite-element modelling.

(Some figures in this article are in colour only in the electronic version)

1. Introduction

The microgripper is an important microsystem component, which is useful in biomedical and biological applications where it can manipulate or isolate individual cells and particles, or carry out localized cell probing and measurement. The requirements for microgrippers for such applications include easy operation, low actuation temperature, low operation voltage and low power consumption. A microgripper actuated by high temperature or high voltage will damage or even kill living cells, limiting its applications. Several efforts have been made to fabricate high performance microgrippers [1–5]. Microtweezers are one type of microgripper, typically made using thin film technology. However, due to thickness limitations, they are incapable of confining micro-objects out of plane [1–3]. Also, micro-tweezers, which capture micro-objects through applying a force directly to the object, may cause damage to the object. A microcage with multiple fingers of a bimorph structure is another type of microgripper [4, 5], which has the advantage of confining and manipulating micro-objects without applying a force directly to the object. However these devices are normally open. A constant power or applied pressure is required to keep the microcage closed during operation. This will increase the temperature of the microcage and the surrounding environment and could damage living cells in a biological experiment. To close these normally open microcages by thermal actuation, extremely high temperatures or very long fingers are needed. In the past,

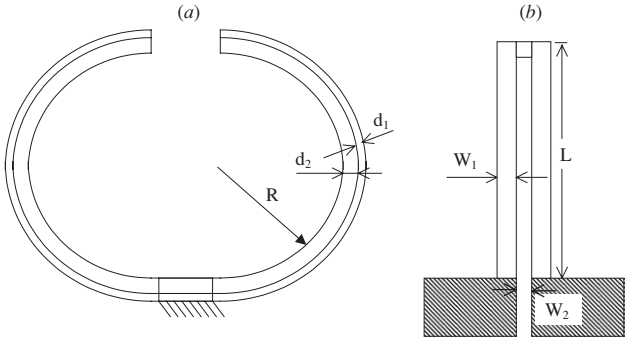

Figure 1. (*a*) A schematic drawing of a bilayer structure microcage containing a highly stressed DLC layer and a stress-free Ni layer. (*b*) The finger configuration of a microcage before release.

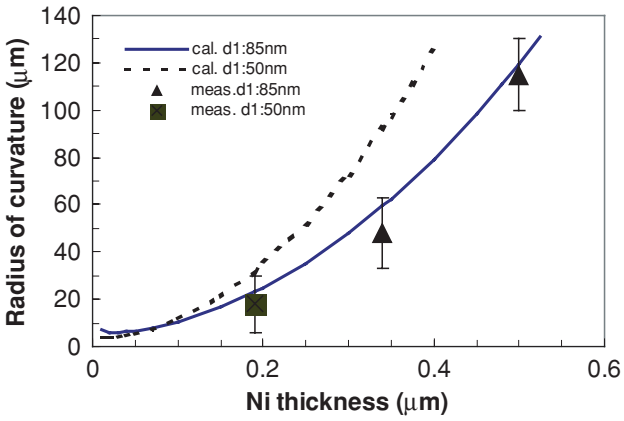

Figure 2. The radius of curvature of a DLC/Ni bilayer as a function of Ni layer thickness for two DLC layers (50 and 85 nm). The discrete points were extracted from the devices made.

the built-in thermal stress of a bimorph layer has been utilized to form pre-curved fingers, but the stress was insufficient to form a small, fully closed microcage [4]. Long fingers were needed to form a closed microcage with a typical diameter of larger than 500 μm. Thus it was unsuitable for biomedical applications. An alternative concept has been developed to make nanotubes from strained semiconductor materials by selectively releasing the strained layers from the substrates [6–8]. The diameter of the nanotubes can be adjusted down to a few tens of nanometres by controlling the overall layer thickness, the strain and the thickness ratio of the top and bottom layers. This technology however has been limited to crystalline materials. Although some progress has been made in the fabrication of microgrippers, there have been no systematic studies of their operation.

Recently we developed normally closed microcages using a diamond-like carbon (DLC) and electroplated Ni bimorph structure by a single mask process [9]. High compressive stress in the amorphous DLC films makes the bimorph structure curl up once it is released from the substrate to form closed microcages with a radius of curvature as small as ~18 μm. This paper provides a comprehensive study of the modelling, fabrication and experimental characterization of these microcages.

2. Theoretical analysis and finite-element simulation

2.1. As-made bimorph structure

The DLC/Ni bimorph structure is firstly analysed using an analytical model. Each bimorph structure, as shown in figures 1(*a*) and (*b*), consists of a compressively stressed DLC layer and a stress-free electroplated Ni layer on top. Once the bimorph structure is released from the substrate, the DLC layer stretches due to its large intrinsic stress, and bends the bimorph layer upwards to form a curved structure. The radius of curvature, R, of such a bimorph structure is given by [10, 11]

$$\frac{1}{R} = \frac{6\,\varepsilon_{\rm eq}(1+m)^2}{d[3(1+m)^2 + (1+mn)(m^2+(mn)^{-1})]} = \varepsilon_{\rm eq}\,S \qquad (1)$$

where $\varepsilon_{\rm eq}$ is the equivalent strain, $d = d_1 + d_2$, with d_1 and d_2 the thicknesses of the DLC and the Ni layer respectively, and n ($= E_1/E_2$) and m ($= d_1/d_2$) the ratios of the Young modulus and the layer thickness. S is a constant for the fixed materials and structural configuration. When $m \sim 1$, it is the most effective bimorph structure to achieve a large deformation, as m approaching zero (one layer dominates the thickness), the bimorph structure behaves as a single-layer structure. For the case of deformation due to a thermal expansion mismatch, the thermal strain is $\varepsilon_{\rm eq}^{\rm th} = (\alpha_1 - \alpha_2)\Delta T$, where α_1 and α_2 are the thermal expansion coefficients and ΔT is the temperature change. $1/R$ is a smooth function of n (or m) at a fixed m (or n). This equation implies that a small radius of curvature can be obtained if two materials with similar Young's moduli are selected. Equation (1) also implies that once the materials and the layer thickness are fixed, the radius of curvature can be adjusted by varying the strain of the DLC layer. This can be achieved through using different deposition methods and/or different process conditions. Assuming the thermal stress of the film is very small due to the low deposition temperature and the stress is uniaxial (since the bimorph is slender), the equivalent strain $\varepsilon_{\rm eq}$ in the DLC layer is related to the as-deposited stress $\sigma_{\rm d}$ and the Young modulus E_1 of the DLC layer, by $\varepsilon_{\rm eq} = \sigma_{\rm d}/E_1$. For a fixed DLC film thickness, the radius of curvature of the bimorph structure can be adjusted by varying the intrinsic stress and the thickness ratio of the two layers. In order to form a closed microcage, the tip of each finger has to curl up by ~180°. This can be realized either by varying the radius of curvature at a fixed finger length, or by adjusting the finger length at a fixed radius of curvature. As demonstrated by other groups [6–8], the best way to make micro-scale curved structures is to reduce the layer thicknesses rather than by introducing in-plane patterning. Figure 2 shows the calculated radius of curvature as a function of Ni layer thickness for two DLC thicknesses (assuming an as-deposited stress of 8 GPa). The radius of curvature increases with increasing Ni thickness, as the fixed force exerted by the thin DLC layer has a reduced ability of deforming the Ni layer. For a fixed Ni thickness, the increase in DLC thickness reduces the radius of curvature. Once the structure and the dimension are fixed, the subtended angle θ (in degrees) of the finger, the so-called tip inclination in beam theory, is related to the finger length L by

$$\theta = 180L/\pi R. \qquad (2)$$

In order to obtain a normally closed microcage (i.e. fingers curled by 180°), the radius of curvature must be in the range

Table 1. Material properties.

	$\alpha(10^{-6}\ \mathrm{K}^{-1})$	$\rho\ (\Omega\ \mathrm{m})$	$k\ (\mathrm{W\ m^{-1}\ K^{-1}})$	E (GPa)	σ (GPa)
Ni	12.7	6.84×10^{-8}	83	205	0
DLC	∼1.0	$>10^{7}$	34	600	8

of $R \sim L/\pi$. For a fixed thickness ratio and required value of R, the angle increases linearly with the finger length. For devices with a DLC thickness in the range of 50–90 nm and Ni thickness of 200–500 nm, a finger length of 100 and 400 μm is needed to make closed microcages.

2.2. Actuation under a voltage

When a current passes through the fingers of a closed microcage, the resistive Joule-heating raises the temperature of the fingers from T_1 to T_2. The Ni layer expands more than the DLC layer due to the difference in thermal expansion coefficients; thus a net thermal compressive strain on the metal side is generated, opening the microcage and changing the radius of curvature from $1/R_1$ to $1/R_2$ correspondingly. The change of the tip inclination can be expressed as

$$\theta_2 - \theta_1 = \frac{180L}{\pi}\left(\frac{1}{R_2} - \frac{1}{R_1}\right) = \frac{180L}{\pi}\Delta\alpha\ \Delta T\ S \qquad (3)$$

where $\Delta\alpha\ \Delta T$ is the thermal strain, generated through the Joule-heating. Assuming that convection and radiation make little contribution to heat losses, the temperature T of the microcage at a steady state is then governed by the basic heat transfer equation [12, 13],

$$k\frac{\mathrm{d}^2T}{\mathrm{d}x^2} + J^2\rho = 0 \qquad (4)$$

$$J = \frac{V}{RA} = \frac{V}{\rho L} \qquad (5)$$

where J is the current density, V the applied voltage, L the length of the resistor, R the resistance, A the cross section of the finger, ρ the resistivity and k is the thermal conductivity.

For a normally closed microcage, it is sufficient to open the fingers only by 90° rather than 180° to capture micro-objects. Using the material properties in table 1, and assuming a finger length of 160 μm and layer thicknesses of 85 nm (DLC) and 340 nm (Ni), it can be shown that a temperature of ∼430 °C is needed to open the fingers by 90°.

Once the structure and materials are fixed, the opening temperature is only determined by $\Delta\alpha$; thus it can be lowered by using a material with a higher thermal expansion coefficient. Metals such as Al and Ni are two of the best candidates for use with the DLC layer. The thermal strain on the Ni side at 430 °C is 0.57%, near half of the DLC compressive strain. This implies that the thermal strain at half of the value of compressive stress in the DLC layer makes the inclination angle of the finger reduce by 50%.

The advantages of using the DLC layer as the bottom layer for this bimorph structure are: (1) the as-deposited DLC films contain large intrinsic compressive stress in the range of 4–10 GPa, which is equivalent to a strain of 0.67–1.67%, similar to those used for nanotubes fabricated from strained semiconductors [6, 7], and this is high enough to form closed microcages with small diameters. (2) The DLC layer has a very low thermal expansion coefficient, $\alpha \sim 1 \times 10^{-6}$ and a combination of a DLC layer and a Ni layer with $\alpha \sim 12.7 \times 10^{-6}$ makes this bimorph device quite efficient during thermal actuation. The DLC layer has good mechanical properties and is biocompatible. As discussed above, a DLC layer with a high compressive stress is essential to form a closed microcage, but the tensile stress on the metal side has a similar function to that of the compressive stress on the DLC, therefore a normally closed microcage can also be obtained from a bilayer of a metal with a high tensile stress and a DLC layer with a low compressive stress. A metal layer with a high tensile stress can easily be obtained by depositing a metal layer at a higher temperature e.g. ∼350 °C, while DLC films grown by other methods such as sputtering and chemical vapour deposition typically have a lower stress of <1 GPa.

Table 2. Summary of device parameters and results.

Parameter name	S1	S2	S3	S4
DLC (nm)	0	85	85	50
Ni (nm)	500	500	340	190
L (μm)	100	200	160	60
Angle (measured °)	0	100	190	190
Angle (calculated °)	0	80	170	180
Angle (FEA °)	0	85	181	185
Radius (measured μm)	∝	115	48	18
Radius (calculated μm)	∝	120	59	32

2.3. Finite-element modelling

In order to validate the analytical simulation presented in section 2.2, finite-element analysis (FEA) based on FEMLAB™ software (a commercially available plug-in software for MATLAB™) was used to model the stress-induced curvatures of the bimorph structures as a function of temperature. A 2D-plane stress model using a parametric nonlinear (large displacement) solution was employed to solve the problem, which allows a bimorph structure with a very large residual stress (e.g. 8 GPa) to be simulated. A step of 0.2 GPa was employed in the simulation. For simplicity, only the constant temperature mode was used in modelling the actuation at an elevated temperature. This is sufficient to compare the simulation with the experimental results. The material properties of the DLC and Ni layers used in the model are listed in table 1.

The curvature was found to be proportional to the stress in the DLC layer as predicted by equation (1). Figure 3(*a*) shows the FEA modelled curvature of a bimorph structure at room temperature with layer thicknesses of DLC/Ni = 85/340 nm, which is similar to device S3 shown in table 2, with a finger length L of 160 μm. It was found that the fingers curled by ∼180° at a compressive stress of 6 GPa for the DLC layer, which is smaller than the value of 8 GPa obtained experimentally. The likely reason for this difference is that the measured stress of the DLC layer included a stress gradient, which was assumed to be zero in the FEA modelling.

Figure 3(*b*) shows the curvature of this device at a temperature of 400 °C, resulting in an open state. The tip inclination of the finger changed from an initial value of 180° at room temperature to ∼90° at 400 °C. Figure 4

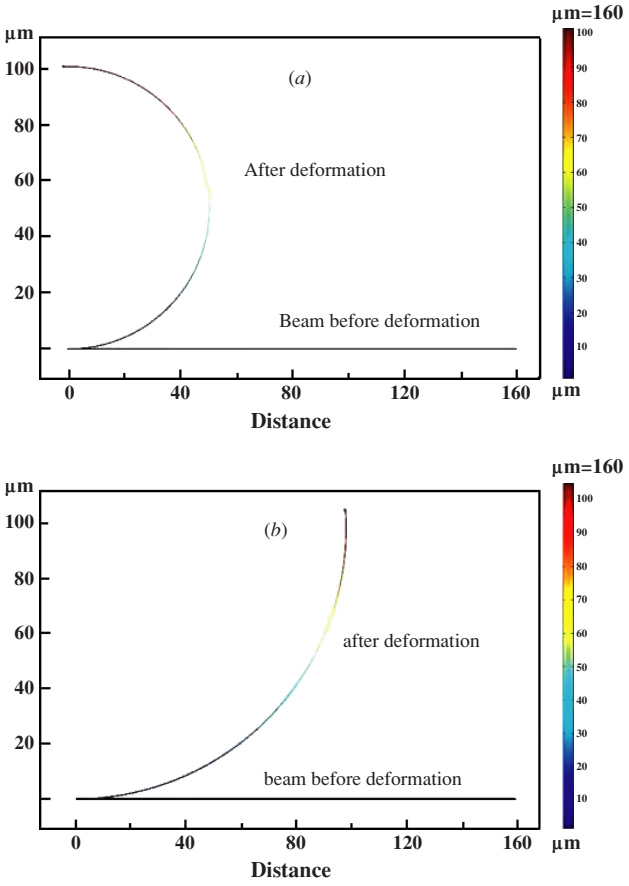

Figure 3. (*a*) The FEA simulation curvature of device S3 with a finger length of $L = 160$ μm. The bimorph layer forms a curvature with an angle of ∼180°. (*b*) The simulated curvature of the same device at a temperature of 400 °C. The vertical bar on the right side is just an indication of deflection of the beam at different sections.

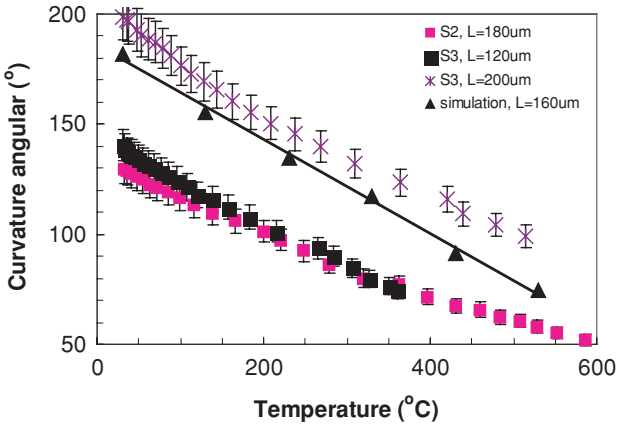

Figure 4. The inclination angle of the finger as a function of temperature for devices S2 and S3. Solid triangles are the FEA simulation results for device S3 with $L = 160$ μm. All devices showed a similar decrease rate in angle as the temperature was increased.

summarizes the results of simulated tip inclination angles as a function of device temperature for device S3, together with the experimental results. The angle of the fingers decreases linearly with increasing temperature, as predicted by equation (3). The full opening temperature (an angle change

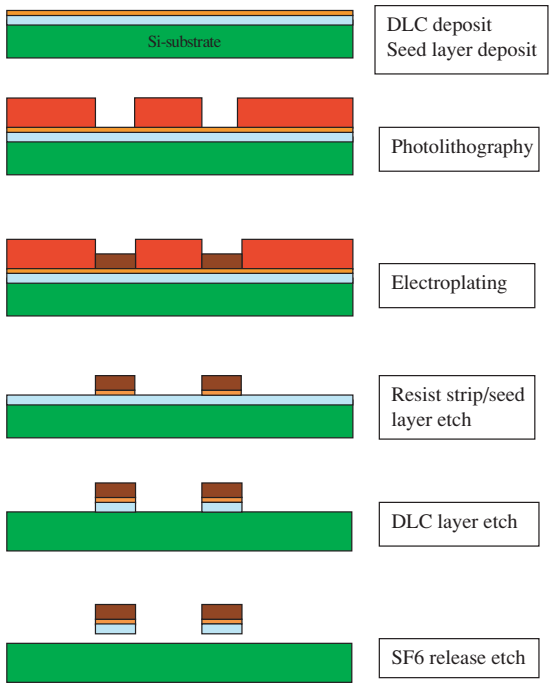

Figure 5. The process flow for the fabrication of a DLC/Ni bimorph microcage.

of 90°) for this device is ∼430 °C, consistent with the value estimated from the analytical model. The tip inclination angle of the finger of the other devices has also been simulated as a function of layer thickness ratios and the results are summarized in table 2. The FEA modelling results are in good agreement with those calculated from the analytical model.

3. Fabrication and testing

The designed microcages use five or six fingers. The width of the metal stripes of the fingers, W_1, and the middle gap between the metal stripes, W_2, are both 4 μm. The fingers are connected to each other electrically and extend to the bond pads. The central part of the grippers is large so that it remains attached to the substrate after the fingers have been released from the substrate. There are four series of devices S1 to S4 with the layer thicknesses shown in table 2. It is worth noting that each series of microcages has several devices with varying finger length from 40 to 200 μm with 20 μm increments. Devices from a particular series (e.g. S3) all have the same thickness ratio as shown in table 2, but with varying finger lengths.

The fabrication process flow is shown in figure 5. It begins with the deposition of the DLC on the Si substrate using the filtered cathodic vacuum arc method [14]. The DLC layer has ∼85% sp^3 bonding[4], with a Young's modulus of ∼600 GPa and a stress ∼8 GPa. The detailed characterization of the DLC films can be found in [14–16]. After deposition, a Cu seed layer with a thickness of ∼50 nm was sputtered on the DLC layer with a ∼5 nm Cr layer to improve the adhesion

[4] sp^2 and sp^3 are the carbon bonds. Carbon films with sp^2 bonds show amorphous properties, while those with sp^3 show diamond properties. A normal DLC film is a mixture of carbons with sp^2 and sp^3 bonds.

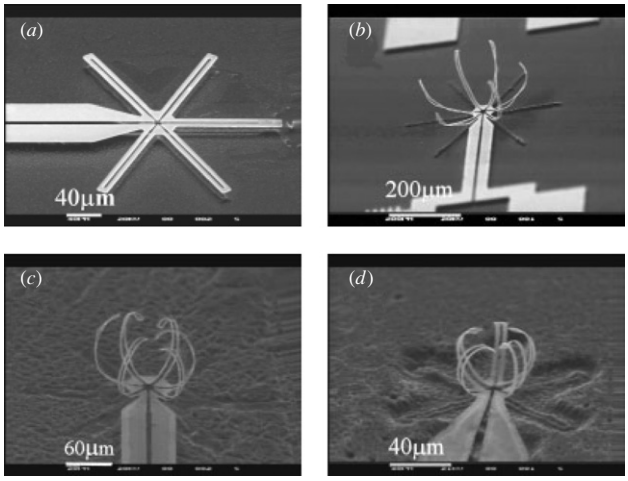

Figure 6. SEM pictures of a single Ni layer S1 (*a*) and bimorph microcages S2–S4. (*b*) DLC/Ni = 85/500 nm, $L = 200$ μm. (*c*) DLC/Ni = 85/340 nm, $L = 160$ μm with an angle of 190°. (d) 50/190, $L = 60$ μm with an angle of 190°.

between the Cu and DLC layers. Optical photolithography was used to form a plating mould using the positive photoresist AZ5214E with a thickness of 1.4 μm. Electroplating was performed in a nickel sulphamate bath at a current of 4 mA cm^{-2} and a temperature of 60 °C. Under optimal conditions, Ni films with low residual stress, high surface quality and Young's modulus of 205 GPa have been obtained [17–19]. After plating, the photoresist and the seed layer outside the active parts were removed by acetone and chromium etchant, respectively. The DLC outside the Ni active area was removed by O_2 plasma etching using patterned Ni as an etching mask. Finally, the microcages were released by SF_6 reactive ion etching to remove the underlying Si. This was controlled by timing so that the central part, the arm strips and the bond pads of the microcages remained attached to the substrate. This ensures that only the fingers of the devices open and close during operation, while other parts do not deform. Also the temperature for these arm strips is much lower than that of the fingers, as wide strips have a low resistance.

The devices were electrically tested at the wafer level on a probe station fixed with a video camera. A Keithley 2400 Source Meter was used to supply the current and to measure the voltage. To minimize the temperature rise of the device, a pulsed mode current with a width of 0.3 s was used. Pictures were taken first under various currents; then were analysed using commercial image analysis software to obtain detailed displacements. Due to the limited magnification of the microscope, the measurements were only carried out for devices with finger lengths larger than 100 μm. Device S4 with closed fingers is too small to be electrically characterized.

4. Results and discussions

4.1. As-made microcage

Figure 6(*a*) shows an SEM picture of a six-finger Ni microcage frame (device S1, without a DLC layer) with a finger length L of 100 μm. The Ni fingers are straight without any curvature visible, indicating there is no stress gradient in the Ni films [17, 19]. Figure 6(*b*) shows an SEM picture of a device S2 microcage with $L = 200$ μm. The fingers curled up with an angle of ∼100°, not sufficient to form a closed cage. This is partially attributed to the Ni top layer being too thick and the finger length being too short. From the analytical model, it is known that a finger length of ∼400 μm is needed for device S2 to form a closed microcage, leading to a size much larger than 100 μm. Figure 6(*c*) is an SEM picture of a six finger microcage (device S3) with a finger length of 160 μm. The fingers curled upwards with an angle of ∼190°, forming a closed microcage with a little over-curvature. The radius of curvature of the fingers is ∼50 μm. This microcage is suitable for capturing micro-objects of sizes 50–100 μm. Smaller microcages can be obtained by further reducing the thickness of the layers. Figure 6(*d*) shows an SEM picture of a five-finger microcage (device S4) with a finger length of 60 μm. The fingers curled up by ∼190°, forming a closed microcage with a radius of curvature of ∼18 μm.

The measured tip inclination and the radii of curvature of these devices with different finger lengths are listed in table 2, together with the corresponding results from the FEA. The extracted radii of curvature of these devices were plotted in figure 2 together with the results from the analytical model. The agreement between the experimental results and the FEA predictions is good, but the difference becomes larger for devices with a thinner DLC layer. The measured radius of curvature $R \sim 18$ μm for device S4 is much smaller than the predicted value of $R \sim 32$ μm. There are several possible reasons for this discrepancy: firstly, in the calculation from the analytical model, the thermal tensile stress caused by an electroplating temperature of 60 °C was not considered. When it was cooled down to room temperature, the contraction of the Ni layer will curl the bimorph structure upwards slightly after being released from the substrate. The thermal tensile stress of the Ni-layer can be estimated to be $\sigma = \Delta\alpha\, \Delta T\, E =$ ∼75 MPa, which is only ∼1% of the DLC film intrinsic stress. Secondly, for the FEA the Cu seed layer was treated as a part of the Ni active material assuming the same Young's modulus value. If a Young's modulus of $E = 128$ GPa is used for the Cu layer, the combined Young's modulus of the bimorph structure becomes smaller. For a Cu seed layer with a thickness of 50 nm, a decrease in combined Young's modulus is found to be ∼5% for device S3 and ∼8% for device S4. Thirdly, the DLC film has a significant through-thickness stress gradient, which typically makes the released layers curl upwards [20]. The stress gradient is normally larger for a thinner film. These factors become significant when the Ni and DLC films become thinner, leading to a large difference between the experimental and calculated results. In addition to these sources of modelling errors, the mechanical properties particular of the DLC cannot be well characterized. The Young modulus value used for the DLC layers was measured using a surface acoustic wave (SAW) method. The accuracy of extracting the Young modulus by various methods including the SAW method is believed to be in the range of 20–30% and is still a research topic for many research groups [21–23]. It is not the exception for the DLC material used here. This may introduce a significant error in estimation of the radius of curvature.

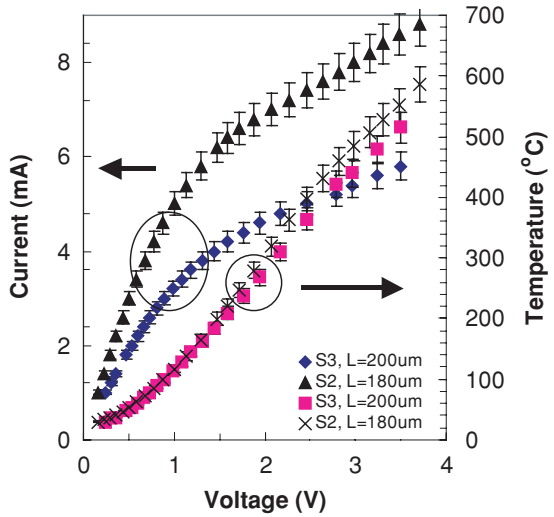

Figure 7. The *I–V* characteristics and the extracted average temperatures as functions of voltage for devices S2 and S3.

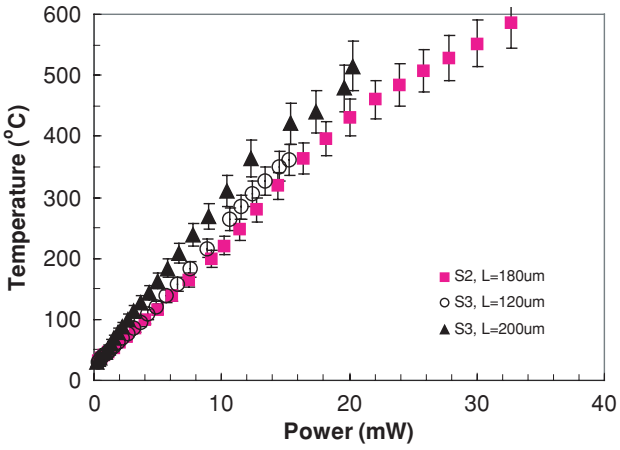

Figure 8. Dependence of the average temperature of the devices on the power consumed for devices S2 and S3.

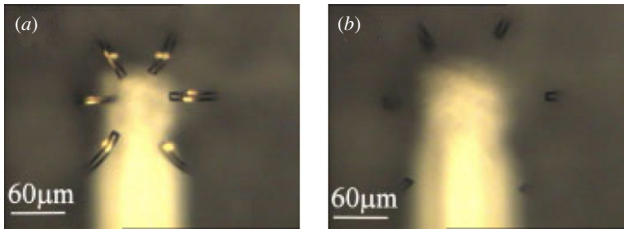

Figure 9. Micrographs of device S3 with a finger length of 160 μm: (*a*) before and (*b*) after applying a pulsed current of 8 mA. The fingers opened laterally by 60 μm on each side.

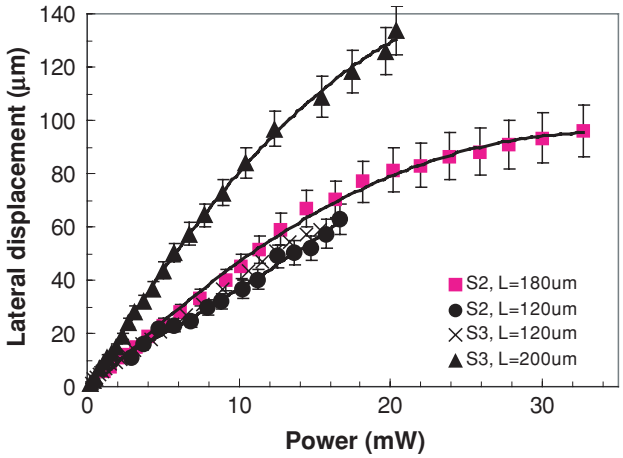

Figure 10. Dependence of the lateral displacement on the power consumed for devices S2 and S3 with different finger lengths.

4.2. Testing under a voltage

A pulsed current can be used to open this type of microcage, rather than supplying a constant current. The resistive Joule-heating generated by a pulse current can be minimized, limiting the rise in the surrounding temperature. From an application point of view, it is also important to know the actual temperature of a working device. The average temperature of a working device can be extracted from the variation of the electrical resistance of the device. To a first-order approximation, the average temperature of a metal resistor can be expressed as

$$T - T_0 = \frac{R(T) - R_0}{\xi R_0}, \tag{6}$$

where ξ is the temperature coefficient of the resistivity, which is 3×10^{-3} K^{-1} for Ni [17], and R_0 is the room temperature resistance of the device. Figure 7 shows the *I–V* characteristics of devices S2 and S3 with finger lengths shown in the figure, demonstrating the typical nonlinear behaviour of metal resistors. The average device temperatures extracted from the variation of the resistances are also shown in figure 7. The average temperatures reached above 500 °C when the voltage was increased above 3 V. Here the parasitic resistances from the probe, contact and cable etc were omitted in the extraction of the device temperatures, as they are only about $2 \pm 0.3\ \Omega$ in total, much smaller than the device resistances. Figure 8 shows the dependence of the extracted average temperatures on power consumed for devices S2 and S3 with different finger lengths. The power was calculated using the current supplied and voltage measured. At low powers, the temperature increases linearly with power, but the rate of increase gradually decreases as the power was further increased. This is believed to be due to the increased heat losses through convection and conduction via the air to the substrate as the temperature increases. A power of only ~20 mW was required to raise the device temperature above 400 °C for all devices.

Figures 9(*a*) and (*b*) are micrographs of a microcage (S3) with a finger length of 160 μm before and after applying a pulsed current of 8 mA. At a power of 16 mW, the fingers of the microcage opened laterally by ~60 μm on each side. Figure 10 summarizes the lateral displacements of the devices as a function of power for devices S2 and S3 with the finger length shown in the figure. At low power, the displacement is proportional to the power consumed. At high power, the rate of increase in displacement gradually decreases and saturates due to the increased heat losses as evidenced in figure 8. It is worth noting that device S2 with $L = 180$ μm and S3 with $L = 120$ μm are not fully closed, but slightly open with an angle of 140 and 130°, while device S3 with $L = 200$ μm was closed with an angle of ~200°.

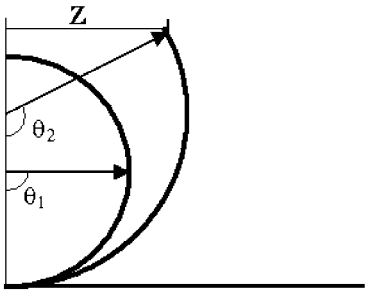

Figure 11. A schematic drawing of a bimorph structure before and after opening.

Since the micrographs were taken from the top of the devices, the lateral displacements are the projections of the curved fingers; thus it is necessary to obtain the subtended angle of the fingers. Figure 11 is a schematic drawing of a bimorph structure. Initially the finger is a semicircle (closed state), and opens with a lateral displacement of Z when the temperature is raised from T_1 to T_2. Assuming the curvature of a bimorph structure is a section (an arc) of a perfect circle with a radius R_1, then the centre of the circles remains on the same vertical line when the temperature is changed as the circle is tangential to the horizon at the finger root. From trigonometry, a relationship between the lateral opening Z and the subtended angle, θ, of the finger can be obtained as follows:

$$\sin(180 - \theta_2) = Z/R_2, \tag{7}$$

as $R_2 = L/\theta_2$, then we obtain

$$\frac{\sin\theta_2}{\theta_2} = \frac{Z\pi}{180L}. \tag{8}$$

From the measured displacement Z, the angle θ of the bimorph structure can be obtained from the plot of $\sin\theta/\theta$ versus θ. The change of angle of the bimorph layers versus the extracted average temperature is shown in figure 4 for devices S2 and S3 with different finger lengths. The inclination of all the devices decreased almost linearly as the temperature was increased. For device S3 with $L = 200$ μm, the initial angle of the finger is $\sim$200° at room temperature. It became $\sim$100° at a temperature of $\sim$500 °C. For device S3 with a finger length of 120 μm, the angle of the finger changed from $\sim$140° to 75° as the temperature was increased from room temperature to $\sim$360 °C. Device S2 had thicker Ni and DLC layers, but it showed a similar behaviour as that of device S3. Also the rates of decrease in the angle with increasing temperature are similar to that obtained from the FEA modelling. Although the initial opening of the devices is different from sample to sample, a temperature rise 400–450 °C is needed to open the microcages by 90°, independent of the thickness ratio, consistent with the estimations from the analytical model and FEA simulation.

It was noted that the devices did not function properly or were burnt once the temperature was increased above 550 °C, probably due to the severe degradation of the nickel and the DLC layers. It is known that the maximum temperature T_{max} of a beam-like resistor is correlated to the average temperature, T_{ave}, by $T_{max} = 1.5\,T_{ave}$ [24]. Therefore for an average temperature of 550 °C, the maximum temperature of the device is more than 800 °C, sufficiently high to damage the DLC layer in air [25] and the Ni layer, and is believed to be responsible for the observation. The reason that the DLC layer actually survived at such a high temperature is due to the pulsed current measurement, which minimized the heating effect on the DLC layer.

The lifetime of the device (S3) has been briefly investigated using a pulsed current with a pulse width of 30 ms. When the device was operated at a temperature lower than 400 °C, there was no detectable degradation in lateral displacement after 10 000 cycles of open/close measurements. When the device was operated at a temperature higher than 450 °C, a significant degradation of the device was observed after testing for more than 1000 cycles with the lateral displacement becoming smaller. This implies that the degradation is caused by the graphitization of the DLC layer at high temperature, rather than the fatigue of the Ni.

Although a pulsed mode actuation can minimize the temperature effect on the environment, the actuation temperature above $\sim$400 °C is too high for biological applications. It is our next target to develop microcages with lower operation temperature. FEA simulations have shown that a microcage with a trilayer of polymer/Al/DLC can be opened at a temperature of $\sim$100 °C. This is under development.

5. Conclusion

A novel normally-closed microcage with small dimensions has been modelled, designed, fabricated and characterized. Analytical and finite-element analyses have been used to simulate the performance of the devices. The devices were made from a highly stressed diamond-like carbon and stress-free electroplated Ni bimorph structure. By adjusting the ratio of the bilayer thickness and the finger length, a normally closed microcage has been demonstrated. The radius of curvature is in the range of 18–50 μm, suitable for capturing and confining micro-objects of sizes 20–50 μm. Analytical and finite-element simulations showed that the devices can be opened by 90° at an elevated temperature of 430 °C. Electrical testing showed that the device can be opened at a power lower than 20 mW, at operation temperatures of $\sim$430 °C. This type of device has the advantage of low power consumption and low operation temperature in a pulsed mode operation.

Acknowledgment

This research was sponsored by the Cambridge-MIT Institute under grant number 059/P.

References

[1] Pan C S and Hsu W Y 1997 An electro-thermally and laterally driven polysilicon microactuator *J. Micromech. Microeng.* **7** 7–13

[2] Roch I, Bidaud Ph, Collard D and Buchaillot L 2003 Fabrication and characterization of an SU-8 gripper actuated by a shape memory alloy thin film *J. Micromech. Microeng.* **13** 330–6

[3] Lee W H, Kang B H, Oh Y S, Stephanou H, Sanderson A C, Skidmore G and Ellis M 2003 Micropeg manipulation with a compliant microgripper *Proc. 2003 IEEE Int. Conf. on Robotics & Automation (Taiwan)* pp 3213–8

[4] Ok J, Chu M and Kim C J 1999 Pneumatically driven microcage for micro-objects in biological liquid *Proc. IEEE Conf. Micro Electro Mechanical Systems (MEMS '99) (Orlando, FL, Jan. 1999)* pp 459–63
[5] Chan H Y and Li W J 2003 A thermally actuated polymer micro robotic gripper for manipulation of biological cells *Proc. 2003 IEEE Int. Conf. on Robotics & Automation (Taipei, Taiwan)* pp 14–9
[6] Prinz V Y, Seleznev V A and Gutakovsky A K 1998 *Proc. 24th Int. Conf. on the Physics of Semiconductors (Israel)* p Th3-D5
[7] Schmidt O G and Jin-Phillipp N Y 2001 Free-standing SiGe-based nanopipelines on Si (0 0 1) substrates *Appl. Phys. Lett.* **78** 3310–2
[8] Vaccaro P O, Kubota K and Aida T 2001 Strain-driven self-positioning of micromachined structures *Appl. Phys. Lett.* **78** 2852–4
[9] Luo J K, Flewitt A J, Spearing S M, Fleck N A and Milne W I 2004 Normally closed microgrippers using highly stressed diamond-like carbon and Ni bimorph structure *Appl. Phys. Lett.* **85** 5748–50
[10] Tsui Y C and Clyne T W 1997 An analytical model for predicting residual stresses in progressively deposited coatings: part 1. Planar geometry *Thin Solid Films* **306** 23
[11] Spearing S M 1997 Design diagrams for reliable layered materials *AIAA J.* **35** 1638–44
[12] Huang Q A and Lee N K S 1999 Analysis and design of polysilicon thermal flexure actuator *J. Micromech. Microeng.* **9** 64–70
[13] Hickey R, Kujath M and Hubbard T 2002 Heat transfer analysis and optimization of two-beam microelectromechanical thermal actuators *J. Vac. Sci. Technol.* A **20** 971–4
[14] Ferrari A C, Kleinsorge B, Morrison N A, Hart A, Stolojan V and Robertson J 1999 Stress reduction and bond stability during thermal annealing of tetrahedral amorphous carbon *J. Appl. Phys.* **85** 7191–8
[15] Polo M C, Andujar J L, Hart A, Robertson J and Milne W I 2000 Preparation of tetrahedral amorphous carbon film by filtered cathodic vacuum arc deposition *Diamond Relat. Mater.* **9** 663–7
[16] Casiraghi C, Ferrari A C, Ohr R, Chu D and Robertson J 2004 Surface properties of altra-thin tetrahedral amorphous carbon films for magnetic storage technology *Diamond Relat. Mater.* **13** 1416–21
[17] Luo J K, He J H, Flewitt A J, Moore D F, Spearing S M, Fleck N A and Milne W I 2004 Development of all metal electro-thermal actuator and its applications *Proc. SPIE* **5344** 201–9
[18] Luo J K, Chu D P, Flewitt A J, Spearing S M, Fleck N A and Milne W I 2005 Uniformity control of Ni thin-film microstructure deposited by through mask plating *J. Electrochem. Soc.* **152** C36–41
[19] Luo J K, Flewitt A J, Spearing S M, Fleck N A and Milne W I 2005 Comparison of microtweezers based on three lateral thermal actuator configurations *J. Microeng. Micromech.* **15** 1294–302
[20] Tsai J T H, Teo K B K and Milne W I 2002 Approach for a self-assembled thin film edge field emitter *J. Vac. Sci. Technol.* B **20** 1–4
[21] Allen M G, Mehregany M, Howe R T and Senturia S D 1987 Microfabricated structures for the *in situ* measurement of residual stress, Young's modulus and ultimate strain of thin films *Appl. Phys. Lett.* **51** 241–3
[22] Zhang J 2002 Determination of Young's modulus of electroplated nickel–ion (Ni/Fe) and micro-machined Si thin films by the balance method *J. Mater. Proc. Technol.* **123** 329–35
[23] Luo J K, Flewitt A J, Spearing S M, Fleck N A and Milne W I 2004 Young's modulus of electroplated Ni thin film fro MEMS applications *Mater. Lett.* **58** 2306–9
[24] Luo J K, Flewitt A J, Spearing S M, Fleck N A and Milne W I 2004 Modelling of microspring thermal actuator *Proc. Nanotech 2004 (Boston)* vol 1 pp 355–8
[25] Zhang Q, Yoon S F, Yang R H and Ahn J 1998 Influence of oxygen on the thermal stability of amorphous hydrogenated carbon film *J. Appl. Phys.* **83** 1349–53